Investigation of Ti Doping on the Structural, Optical and Magnetic Properties of ZnO Nanoparticles

Raji P
Mepco Schlenk Engineering College
K Balachandra Kumar (dkbaldr@gmail.com)
Government Arts and Science College https://orcid.org/0000-0003-0659-6629

Research Article

Keywords: ZnO, Coprecipitation, XRD, SEM, FTIR, VSM

Posted Date: February 9th, 2021

DOI: https://doi.org/10.21203/rs.3.rs-171786/v1

Version of Record: A version of this preprint was published at Journal of Materials Science: Materials in Electronics on April 12th, 2021. See the published version at https://doi.org/10.1007/s10854-021-05803-y.

Investigation of Ti doping on the structural,optical and magnetic properties of ZnO nanoparticles

P. Raji[1] and K.Balachandra Kumar[2*]

[1]Department of Physics, Mepco Schlenk Engineering College, Sivakasi- 626005

[2]Department of Physics, Government Arts and Science College, Sivakasi - 626124

ABSTRACT

Ti - doped ZnO ($Ti_xZn_{1-x}O$ x= 0.00, 0.05, 0.10, 0.15) nanoparticles have been synthesized through co - precipitation approach. X-ray diffraction (XRD), scanning electron microscopy (SEM), photoluminescence (PL), UV-Visible spectroscopy, and Vibrating Sample Magnetometer (VSM) have been used to characterize the samples. X-Ray Diffraction (XRD) analysis manifested the hexagonal wurtzite structure. The crystallite size decreased from 37 nm to 29 nm as dopant concentration is increased. Fourier transform infrared analysis showed the absorption bands of ZnO, with few within the intensities. SEM investigation showed the irregular shape and agglomeration of the particles. Ti, Zn, and O composition were determined from EDX analysis and confirmed the purity of the samples.PL spectra showed a near band edge emission and visible emission.Vibrating sample magnetometer (VSM) demonstrated pure and doped samples exhibited ferromagnetism behavior at room temperature.

Keywords: ZnO; Coprecipitation; XRD; SEM; FTIR; VSM.

Corresponding Author Email: dkbaldr@gmail.com

1. Introduction:

In recent years, semimagnetic semiconductors (SMSs) have attracted significant interest because of their versatile capability packages in spintronics devices [1–4]. They had been generally acquired by doping a small amount of Transition metallic (TM: Fe, Co,Ni, Mn, Cr, and so on.) into semiconductors.

In Diluted Magnetic oxides, ferromagnetism at room temperature (RTFM) observed may be due to the intrinsic defects (oxygen vacancies) or presence of secondary phases (extrinsic) and it depends on the methods of preparation. Among II - VI semiconductors, Zinc oxide has a large excitation binding energy (60 meV) with wide direct bandgap [5,6] . Still, there are a lot of requirements to enlighten the origin of the RTFM in Transition metal doped ZnO.

Among Transition metals [7-10], Titanium can be easily substituted for host ions due to its d subshells filled in partial. It is a non - ferromagnetic element with a lesser bond length, ionic radius and more valency electron compared with Zn [11]. Hence, Ti is a suitable transition metal compared with other materials . The properties of ZnO nanoparticles could be easily changed and controlled by doping with Ti.

Venkatesan *et al*. [12] and Antony *et al*. [13] synthesized Ti doped ZnO films exhibited room temperature Ferromagnetism with a saturation moment of about 0.15μB/Ti. Akilan *et.al*. [14] reported defects induced room temperature ferromagnetism in Ti doped ZnO prepared by solid state reaction method .

Various techniques such as radio-frequency (RF) magnetron sputtering , pulsed laser deposition , chemical vapor deposition (CVD), atomic layer deposition (ALD), have been used to

prepare Ti-doped ZnO thinfilm [15-17]. Besides , some reports on Ti doped ZnO nanomaterials by sol gel and ball milling [18,19].

To the best of our knowledge, there are no reports on Ti doped ZnO nanopowders by co-precipitation carried out so far. It has the advantages of a simple , low cost, easy modification of dopant concentration , controlled particle size and bulk scale synthesis of nanoparticles [20].

In this article, we focus on the synthesis of Ti doped ZnO nanoparticles by co - precipitation method. Influence of Ti doping on structural , optical and magnetic properties of ZnO nanoparticles have been studied by x-ray diffraction (XRD) method, Fourier transform infrared (FTIR)spectroscopy, Ultraviolet–visible (UV–vis) spectroscopy, Photoluminescence (PL) spectroscopy, Scanning electron microscopy (SEM) with compositional analysis and vibrational sample magnetometer (VSM).

2. Materials and Methods

2.1 Synthesis of undoped and Ti doped ZnO nanoparticles:

Analytical reagent chemicals Zinc chloride($ZnCl_2 \cdot 2H_2O$) ,Titanium tetraChloride ($TiCl_4$) and Sodium hydroxide (NaOH) were purchased from Merck used as the starting materials for Zn, Ti and OH and used as received. Pure ZnO and Ti doped ZnO nanoparticles were synthesized by simple precipitation method.

Initially, Zinc chloride and Titanium tetrachloride were dissolved separately in 100 mL of pure distilled water to make 0.2 M of solution . These two solutions are mixed with each other in a stoichiometric ratio under magnetic stirring for 30 minutes. Then, sodium hydroxide solution was added to the above mixture drop by drop and stirred continuously. The addition of

sodium hydroxide was stopped until pH = 13, and stirring was continued for 2 h. It was observed that white precipitation continued to be formed. The white precipitate was washed repeatedly with deionized water and absolute ethanol to remove impurities. Then the precipitate was dried at 150 °C for 2 h and the dried powder was calcined in air at 600 °C for 5 h.

2.2. Characterization:

The phase structure and crystalline size of the samples were determined by X-Ray diffraction (XRD) using a PANalytical X'pertPro diffractometer with Cu-Kα radiation (wavelength of 1.5406 Å) . The surface morphology of the samples were studied by SEM (Carl Zeiss SUPRA-55). UV–vis absorption spectra of all the samples were recorded by Shimadzu-UV 2450 spectrophotometer. The photoluminescence (PL) measurements were carried out by Perkin Elmer-LS 45 spectrofluorometer with an excitation wavelength 325 nm. Fourier transformed infrared (FTIR) spectra of the samples were recorded using a Shimadzu-FTIR spectrometer and room temperature magnetic measurements were obtained by LAKESHORE-7410 vibrating sample magnetometer (VSM).

3. Results and discussion:

3.1. Structural characterization

Fig. 1 shows the XRD pattern for undoped and Ti doped ZnO (x= 0.05, 0.10, 0.15) nanoparticles.It shows well crystalline single phase wurtzite structure (space group p63mc, JCPDS No:36-1451) .The XRD pattern have diffraction peaks at ~ 31.6°, 33.2°, 36.3°, 47.8°, 56.5°, 62.2°, 66.1°, 67.7°, 69.5° corresponds to (100), (002), (101), (102), (110), (103) , (112) (200) and (201) planes. The intensities of peaks continuously decrease with Ti doping

indicates that Ti^{4+} ions (ionic radius: 0.068nm) are substituted in Zn^{2+} ions (ionic radius: 0.074nm) [22].

From the d spacing values, the lattice constant '*a*' and '*c*' can be calculated [21] and their values are given in Table 1.

$$\frac{1}{d^2}=\frac{4\left(h^2+hk+k^2\right)}{3a^2}+\frac{l^2}{c^2} \quad (1)$$

where 'h', 'k' and 'l' are miller indices, 'a' and 'c' are lattice parameters, and 'd' is the inter planner spacing. The lattice constant values are found slightly lower than the standard values of a = 3.2498 Å and c = 5.2066 Å (JCPDS card no: 36-1451). The lattice parameters (a and c) and microstrain of the samples considerably increased with increasing Ti concentration [23] .

The average crystallite size of the sample was calculated by using Debye - scherrer's formula [21].

$$D=\frac{0.89\lambda}{\beta\cos\theta} \quad (2)$$

where, λ is the wavelength of X-ray (1.54Å), β is the full width at half maximum and θ is the angle of diffraction. The average crystallite size was found to be 37.46 nm for ZnO and it decreased to 29.36 nm for 15% Ti doped ZnO. The decrease in the crystallite size is mainly due to the doped Ti^{4+} ions that reduce nucleation and rate of growth of ZnO NPs.

The dislocation density is calculated by using the following relation [21],

$$\delta_{(hkl)}=\frac{1}{t_{DS}^2}$$

The dislocation density indicates the crystallinity of a crystal, and it will increase with increasing Ti concentration.

By using the following equation, the volume of the unit cell is calculated [21].

$$V = 0.866a^2c$$

Atomic packing fraction (APF) is estimated using the formula [21],

$$APF = \frac{2\pi a}{3\sqrt{3}c}$$

The value of APF does not change from that for bulk ZnO sample and this means that the doping of Ti to ZnO has not created new voids .

The atomic displacements 'u' is given as [21],

$$u = \frac{a^2}{3c^2} + \frac{1}{4}$$

The average bond length between the cations and the anions can be calculated by the following expression [21].

$$L = \sqrt{\left(\frac{a^2}{3}\right) + \left(\frac{1}{2} - u\right)c^2}$$

3.2 Estimation of Young's modulus & Energy density:

The Young's modulus, energy per unit volume of a lattice (u) and stress (σ) can be calculated by the following expressions [24]

$$Y = \frac{\left(h^2 + \frac{(h+2k)^2}{3} + \left(\frac{al}{c}\right)^2\right)^2}{S_{11}\left(h^2 + \frac{(h+2k)^2}{3}\right) + S_{33}\left(\frac{al}{c}\right)^4 + (2S_{13} + S_{44})\left(h^2 + \left(\frac{h^2+2k}{3}\right)\right)\left(\frac{al}{c}\right)^2}$$

$$u = \frac{\varepsilon^2 Y}{2}$$

$$\sigma = Y\varepsilon$$

Here S_{11}, S_{13}, S_{33},S_{44} are the elastic constants of ZnO. The values of the constants are 7.588 x 10^{-12} m^2N^{-1} , 2.206 x 10^{-12} m^2N^{-1}, 6.94 x 10^{-12} m^2N^{-1} , 23.57 x 10^{-12} m^2N^{-1} respectively.

The value of Young's modulus, energy density and stress of the NPs are calculated and tabulated (Table 1). It is observed that the energy density increases when the percentage of Ti increases .

3.3 MORPHOLOGICAL ANALYSIS

Figure 2 shows SEM images of pure and Ti doped ZnO nanoparticles. Random agglomeration with cluster shape were observed in all SEM images .

3.4.FOURIER TRANSFORMED INFRARED SPECTROSCOPY (FTIR)

Figure 3 represents the FTIR spectra for undoped and Ti doped ZnO nanoparticles. The srtong absorption band observed at 3500 cm^{-1} is owing to the stretching vibration of [O – H in water molecules [25].The presence of CO_2 molecules is confirmed by the absorption band at 2300 cm^{-1} [26]. A sharp absorption band at 1600 cm^{-1} is ascribed to bending vibration of H–O–H [27]. The band observed at 1400cm^{-1} is owing to OCO group asymmetric (C=O) and symmetric (C-O) stretching vibrations. [28]. The band at 465 cm^{-1} is due to stretching frequency of Zn-O [29] and it is shifted to a low frequency mode with increasing doping concentration. The change in frequency is observed because of change in bond length due to addition of Ti in ZnO.

3.5 UV -Vis spectroscopy

The optical absorption properties of undoped ZnO and Ti doped samples were analysed using UV-VIS spectrometer. The bandgap of undoped and Ti doped ZnO nanoparticles was calculated by Tauc's plot using the relation

$$\alpha h\nu = B\,(h\nu - Eg)^{n} \qquad (3)$$

where α - absorption coefficient , B - constant, h - Planck's constant, ν - photon frequency, and E_g is the optical band gap.

The energy bandgap of ZnO and Ti -doped ZnO nanoparticles were found to be 3.25, 3.28, 3.4, and 3.67eV, respectively (Fig.4). The redshift in the bandgap is due to the Burstein-Moss effect [30]. The conduction band lower levels are filled with free electrons generated When Ti^{4+} ions replace the Zn^{2+} ions . Subsequently, it increase the Fermi Level and also widening the band gap , [31]. According to quantum confinement effect, the smaller crystallites have a larger bandgap in metal oxide systems [32]. This is correlated with the findings in the XRD section in which the crystallite size of ZnO nanoparticles is reduced with the addition of Ti.

3.6. Photoluminescence (PL)

Figure 5 shows Room temperature PL emission spectra of undoped ZnO, 5% , 10%,15% Ti doped ZnO samples. Technically, all the samples were excited at 325 nm.It is noticed that undoped and doped ZnO samples exhibits two peaks (i) 390nm (UV range) originates from the exciton recombination corresponding to the near-band edge (NBE) and (ii) 412nm (violet range), to be the recombination from the defect centerssuch as O and Zn interstitials.

Defects such as structural defects or vacancies is the main reason for the emission of different deep-trap or colors [34] . Interstital zinc ond oxygen are ascribed to structural defects

while vacancies are produced due to the presence of Zinc and oxygen vacancy [35]. High content of zinc vacancy is the main reason for the violet emission peak observed at 418 nm [36].

3.7. Magnetic property:

Pure and Ti doped ZnO samples magnetic properties were studied at room temperature shown in Figure 6. All samples are ferromagnetic as observed from the M-H hysteresis loops and the values are give in Table 2 . The plots of coercivity and retentivity as a function of dopant concentration are shown for all the samples. The trends of variations are nearly similar to those of dislocations density as a function of dopant concentration.

The room temperature ferromagnetism of the nanoparticles could arise due to extrinsic magnetism or intrinsic magnetism. But no traces of impurity or secondary phases in XRD ruled out the RTFM due to extrinsic source. Hence, the attained ferromagnetism is an intrinsic magnetic property of the nanoparticles. The bound magnetic polarons (BMPs) theoretical model [37] is a defect-induce ferromagnetism model. According to this, the ferromagnetism arises due to the oxygen vacancies and dopant ions indirect interaction. The stable ferromagnetic interaction arises due to extend over of polarons. Exchange interaction between oxygen vacancies or interstitial Zn atom withoverlap of 3d orbital electrons in ZnO nanoparticles is the origin of Ferromangetism [38]. The PL results also suggested the oxygen vacancies in ZnO. As the presence of such defects is not huge, the extent of ferromagnetic ordering and hence coercivity is relatively week.

Conclusions

Ti doped ZnO nanoparticles were successfully synthesized by co precipitation technique. From XRD, it is found that our samples are having single phase hexagonal wurtzite structure and the average crystallite size 37-29 nm. Scanning Electron Microscopic investigation revealed the morphology of pure ZnO and 5%, 10% and 15% nano particle seemed to be approximately spherical in shape. The EDX spectrum confirmed the presence of Ti in ZnO nanoparticles. Fourier Transform Infrared spectra were recorded to analyze the effect of Ti doping on the nanoparticles. The UV-visible spectroscopic study the intercepts yield the direct energy band for the Ti doped ZnO 5%, 10% and 15% samples are 3.25 3.28 and 3.4 eV respectively. Room temperature VSM study demonstrates that all the samples are suitable for spintronic applications.

Conflict of interest statement

On behalf of all authors, the corresponding author states that there is no conflict of interest.

References

1 Dietl, Tomasz. "Ferromagnetic semiconductors." *Semiconductor Science and Technology* 17.4 (2002): 377 - 392.

2 Akinaga, Hiro, and Hideo Ohno. "Semiconductor spintronics." *IEEE Transactions on nanotechnology* 1.1 (2002): 19-31.

3 Pearton, S. J., Abernathy, C. R., Overberg, M. E., Thaler, G. T., Norton, D. P., Theodoropoulou, N. & Boatner, L. A. (2003). Wide band gap ferromagnetic semiconductors and oxides. *Journal of Applied Physics*, *93*(1), 1-13.

4 Malajovich, I., Berry, J. J., Samarth, N., & Awschalom, D. D. (2001). Persistent sourcing of coherent spins for multifunctional semiconductor spintronics. *Nature*, *411*(6839), 770-772.

5 Jin, Z., Fukumura, T., Kawasaki, M., Ando, K., Saito, H., Sekiguchi, T., ... & Koinuma, H. (2001). High throughput fabrication of transition-metal-doped epitaxial ZnO thin films: A series of oxide-diluted magnetic semiconductors and their properties. *Applied Physics Letters*, *78*(24), 3824-3826.

6 Ueda, K., Tabata, H., & Kawai, T. (2001). Magnetic and electric properties of transition-metal-doped ZnO films. *Applied Physics Letters*, *79*(7), 988-990.

7 Ahmadipour, M., Hatami, M., & Sadabadi, H. (2013). Magnetic property of Zn0. 8CO0. 2O diluted magnetic semiconductors by auto combustion method. *Int J Curr Eng Technol*, *3*(1), 85.

8 Yong, Z., Liu, T., Uruga, T., Tanida, H., Qi, D., Rusydi, A., & Wee, A. T. (2010). Ti-doped ZnO thin films prepared at different ambient conditions: electronic structures and magnetic properties. *Materials*, *3*(6), 3642-3653.

9 Shao, Q., Wang, C., Zapien, J. A., Leung, C. W., & Ruotolo, A. (2015). Ferromagnetism in Ti-doped ZnO thin films. *Journal of Applied Physics*, *117*(17), 17B908.

10 Zheng, K., Gu, L., Sun, D., Mo, X., & Chen, G. (2010). The properties of ethanol gas sensor based on Ti doped ZnO nanotetrapods. *Materials Science and Engineering: B*, *166*(1), 104-107.

11 Huang, H., Liu, Y., Wang, J., Gao, M., Peng, X., & Ye, Z. (2013). Self-assembly of mesoporous CuO nanosheets–CNT 3D-network composites for lithium-ion batteries. *Nanoscale*, *5*(5), 1785-1788.

12 Venkatesan, M., Fitzgerald, C. B., Lunney, J. G., & Coey, J. M. D. (2004). Anisotropic ferromagnetism in substituted zinc oxide. *Physical review letters*, *93*(17), 177206.

13 Antony, J., Pendyala, S., McCready, D. E., Engelhard, M. H., Meyer, D., Sharma, A., & Qiang, Y. (2006). Ferromagnetism in Ti-doped ZnO nanoclusters above room temperature. *IEEE transactions on magnetics*, *42*(10), 2697-2699.

14 Akilan, T., Srinivasan, N., & Saravanan, R. (2015). Magnetic and optical properties of Ti doped ZnO prepared by solid state reaction method. *Materials Science in Semiconductor Processing*, *30*, 381-387.

15 Shewale, P. S., Lee, N. K., Lee, S. H., Kang, K. Y., & Yu, Y. S. (2015). Ti doped ZnO thin film based UV photodetector: Fabrication and characterization. *Journal of Alloys and Compounds*, *624*, 251-257.

16 Jamil, A., Fareed, S., Tiwari, N., Li, C., Cheng, B., Xu, X., & Rafiq, M. A. (2019). Effect of titanium doping on conductivity, density of states and conduction mechanism in ZnO thin film. *Applied Physics A*, *125*(4), 238.

17 Ye, Z. Y., Lu, H. L., Geng, Y., Gu, Y. Z., Xie, Z. Y., Zhang, Y., ... & Zhang, D. W. (2013). Structural, electrical, and optical properties of Ti-doped ZnO films fabricated by atomic layer deposition. *Nanoscale research letters*, *8*(1), 1-6.

18 Yilmaz, M., & Turgut, G. Ü. V. E. N. (2015). Titanium doping effect on the characteristic properties of sol-gel deposited ZnO thin films. *Kovove Mater*, *53*, 333-339.

19 Suwanboon, S., Amornpitoksuk, P., & Bangrak, P. (2011). Synthesis, characterization and optical properties of Zn1− xTixO nanoparticles prepared via a high-energy ball milling technique. *Ceramics International*, *37*(1), 333-340.

20 Muthukumaran, S., & Gopalakrishnan, R. (2012). Structural, FTIR and photoluminescence studies of Cu doped ZnO nanopowders by co-precipitation method. *Optical Materials*, *34*(11), 1946-1953.

21 Singhal, S.; Kaur, J.; Namgyal, T.; Sharma, R. Cu-Doped ZnO Nanoparticles: Synthesis, Structural and Electrical Properties. Physica B 2012, 407, 1223−1226

22 Gandhi, V., Ganesan, R., Abdulrahman Syedahamed, H. H., & Thaiyan, M. (2014). Effect of cobalt doping on structural, optical, and magnetic properties of ZnO nanoparticles synthesized by coprecipitation method. *The Journal of Physical Chemistry C*, *118*(18), 9715-9725.

23 Darmadi, I., Taufik, A., & Saleh, R. (2020, January). Analysis of optical and structural properties of Ti-doped ZnO nanoparticles synthesized by co-precipitation method. In *Journal of Physics: Conference Series* (Vol. 1442, No. 1, p. 012021). IOP Publishing.

24 Sundaram, P. S., Inbanathan, S. S. R., & Arivazhagan, G. (2019). Structural and optical properties of Mn doped ZnO nanoparticles prepared by co-precipitation method. *Physica B: Condensed Matter*, *574*, 411668.

25 I. Khan, S. Khan, R. Nongjai, H. Ahmed, W. Khan, Structural and optical properties of gel combustion synthesized Zr doped ZnO nanoparticles, Optic. Mater. 35 (2013) 1189-1193.
26 E. Indrajith Naik, H. S. Bhojya Naik, R. Viswanath, I. K. Suresh Gowda, M. C. Prabhakara, Bright red luminescence emission of macroporous honeycomb-like Eu3+ ion-doped ZnO nanoparticles developed by gel-combustion technique, SN Applied Sciences 2 (2020) 863 -867.
27 Naik, E. I., Naik, H. B., Viswanath, R., Kirthan, B. R., & Prabhakara, M. C. (2020). Effect of zirconium doping on the structural, optical, electrochemical and antibacterial properties of ZnO nanoparticles prepared by sol-gel method. *Chemical Data Collections*, 100505 - 100511.
28 Josepha Foba-Tendo, Lambi John Ngolui, Beckley Victorine Namondo, Fomogne Cyrille Yollande, and Marius Borel Nguefack Nguimezong, Structural Characterization and Magnetic Properties of Undoped and Ti-Doped ZnO Nanoparticles Prepared by Modified Oxalate Route, Volume 2018 |Article ID 9072325
29 A. Sohail, M. Faraz, H. Arif, S.A. Bhat, A.A. Siddiqui, B. Bano, Deciphering the interaction of bovine heart cystatin with ZnO nanoparticles: Spectroscopic and thermodynamic approach, Int. J. Biol. Macromol. 95 (2017) 1056-1063.
30 N.C.S. Selvam, J.J. Vijaya, L.J. Kennedy, Effects of Morphology and Zr Doping on Structural, Optical, and Photocatalytic Properties of ZnO Nanostructures, Ind. Eng. Chem. Res. 51 (2012) 16333-16345.
31 P.V. Rajkumar, K. Ravichandran, K. Karthika, B. Sakthivel, B. Muralidharan, Enhancement of electrical conductivity of sol–gel doped ZnO films through Zr doping and vacuum annealing, Mater. Pro. Rep. 31 (2015) 234 - 240.
32 D. Fang, C. Li, N. Wang, P. Li, P. Yao, Structural and optical properties of Mg-doped ZnO thin films prepared by a modified Pechini method, Cryst. Res. Technol. 48 (2013) 265-272.
33 K.P. Shinde, R.C. Pawar, B.B. Sinha, H.S. Kim, S.S. Oh, K.C. Chung, Optical and magnetic properties of Ni doped ZnO planetary ball milled nanopowder synthesized by coprecipitation, Ceram. Intern. 40 (2014) 6799-16804.
34 L. Duan, X. Zhao, Y. Wang. W. Geng, F. Zhang, Structural and optical properties of (Mg, Al)-codoped ZnO nanoparticles synthesized by the autocombustion method, Ceram. Int. 41 (2015) 6373-6380.
35 U. Godavarti, V.D. Mote, M.V. Ramana Reddy, P. Nagaraju, Y. Vijaya Kumar, K.T. Dasari, M.P. Dasari, Precipitated cobalt doped ZnO nanoparticles with enhanced low temperature xylene sensing properties, Physica B. 553 (2019) 151-160.
36 Khenfouch, M., Baïtoul, M., & Maaza, M. (2012). White photoluminescence from a grown ZnO nanorods/graphene hybrid nanostructure. *optical Materials*, *34*(8), 1320-1326.

37 Hsu, H. S., Huang, J. C. A., Huang, Y. H., Liao, Y. F., Lin, M. Z., Lee, C. H., & Liu, C. P. (2006). Evidence of oxygen vacancy enhanced room-temperature ferromagnetism in Co-doped ZnO. *Applied Physics Letters*, *88*(24), 242507.

38 Iqbal, J., Wang, B., Liu, X., Yu, D., He, B., & Yu, R. (2009). Oxygen-vacancy-induced green emission and room-temperature ferromagnetism in Ni-doped ZnO nanorods. *New Journal of Physics*, *11*(6), 063009 – 063014.

Figures

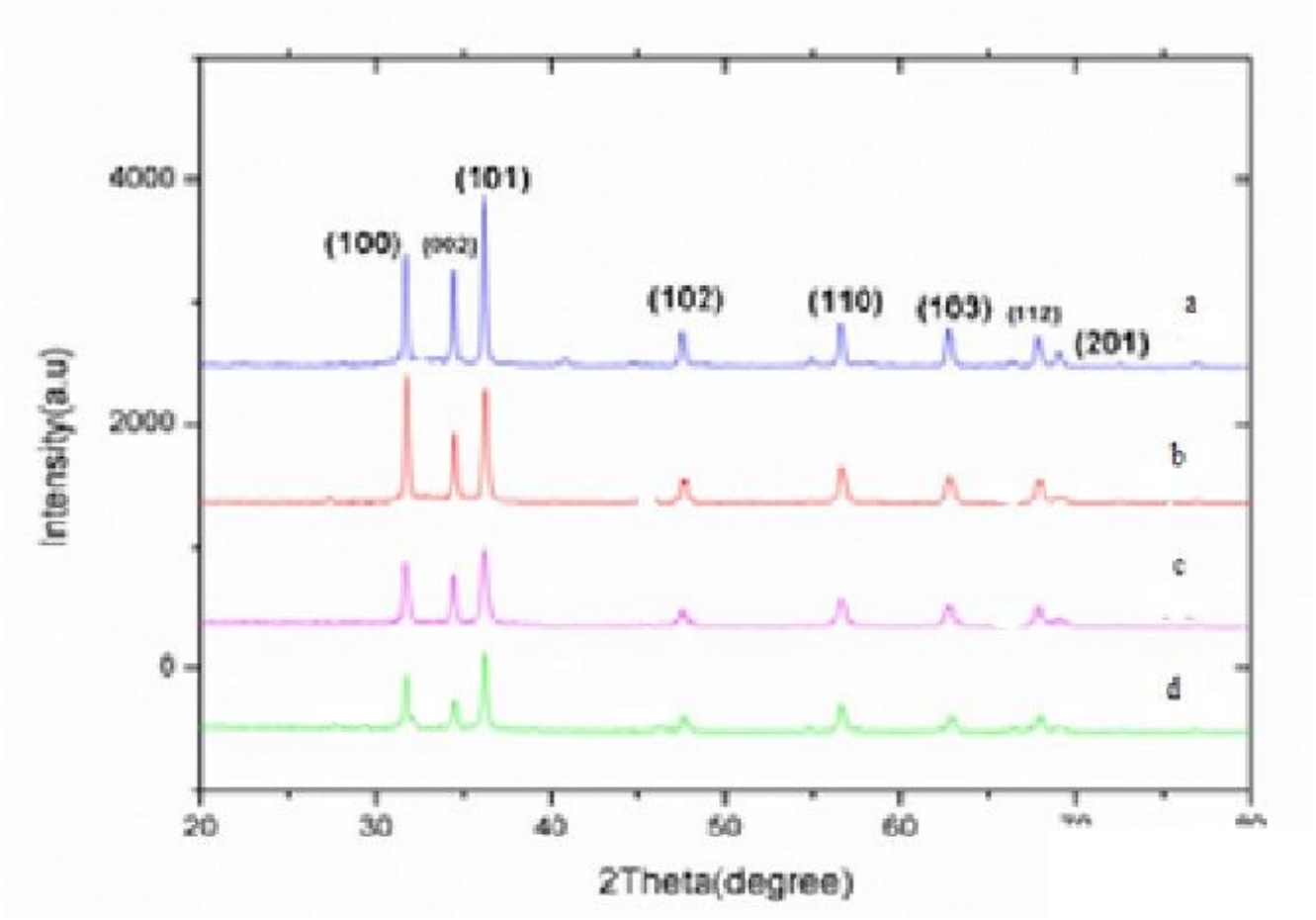

Figure 1

XRD pattern of Ti x Zn1-xO (x= 0,0.05, 0.10,& 0.15)

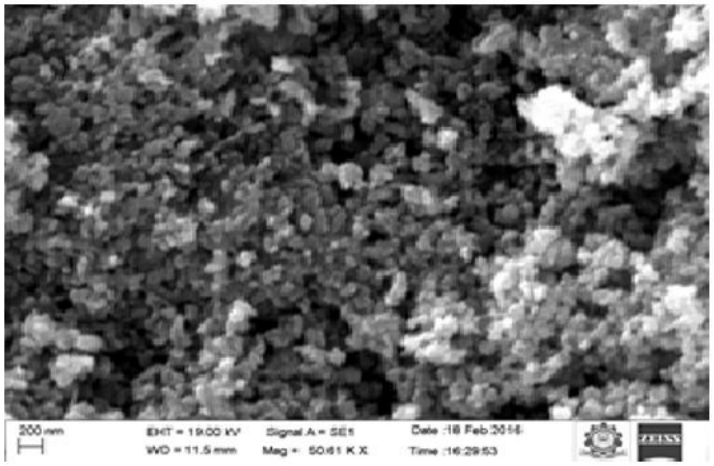

(a) doped ZnO

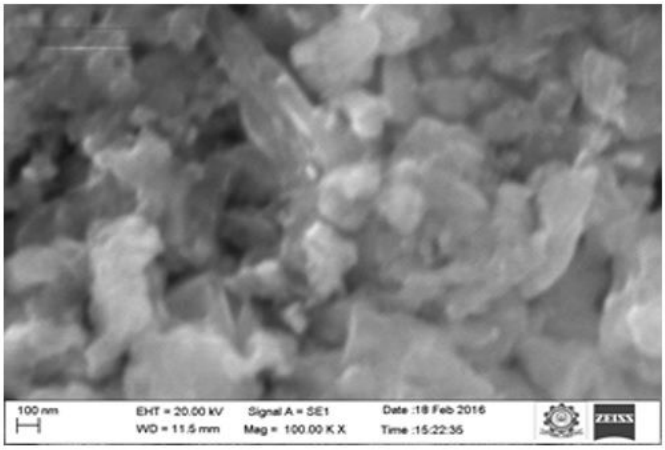

(c) 10 % Ti doped ZnO

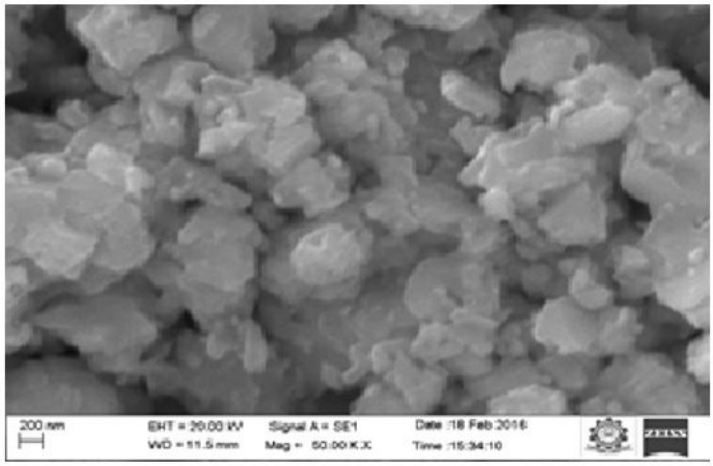

(b) 5% Ti doped ZnO

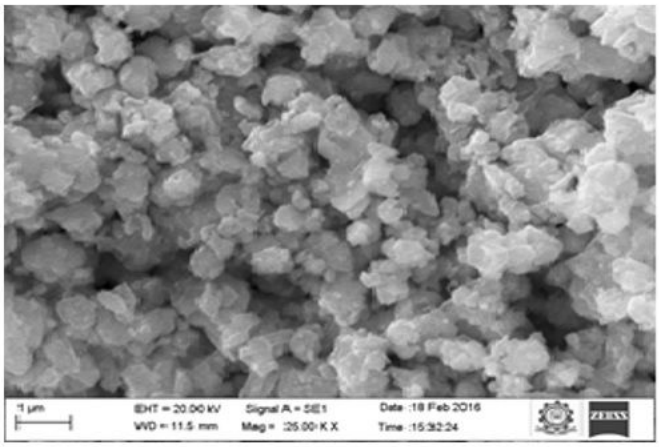

(d) 15% Ti doped ZnO

Figure 2

SEM images for (a) undoped ZnO, (b) 5 % Ti doped, (c) 10% Ti-doped and (d) 15% Ti-doped ZnO nanoparticles.

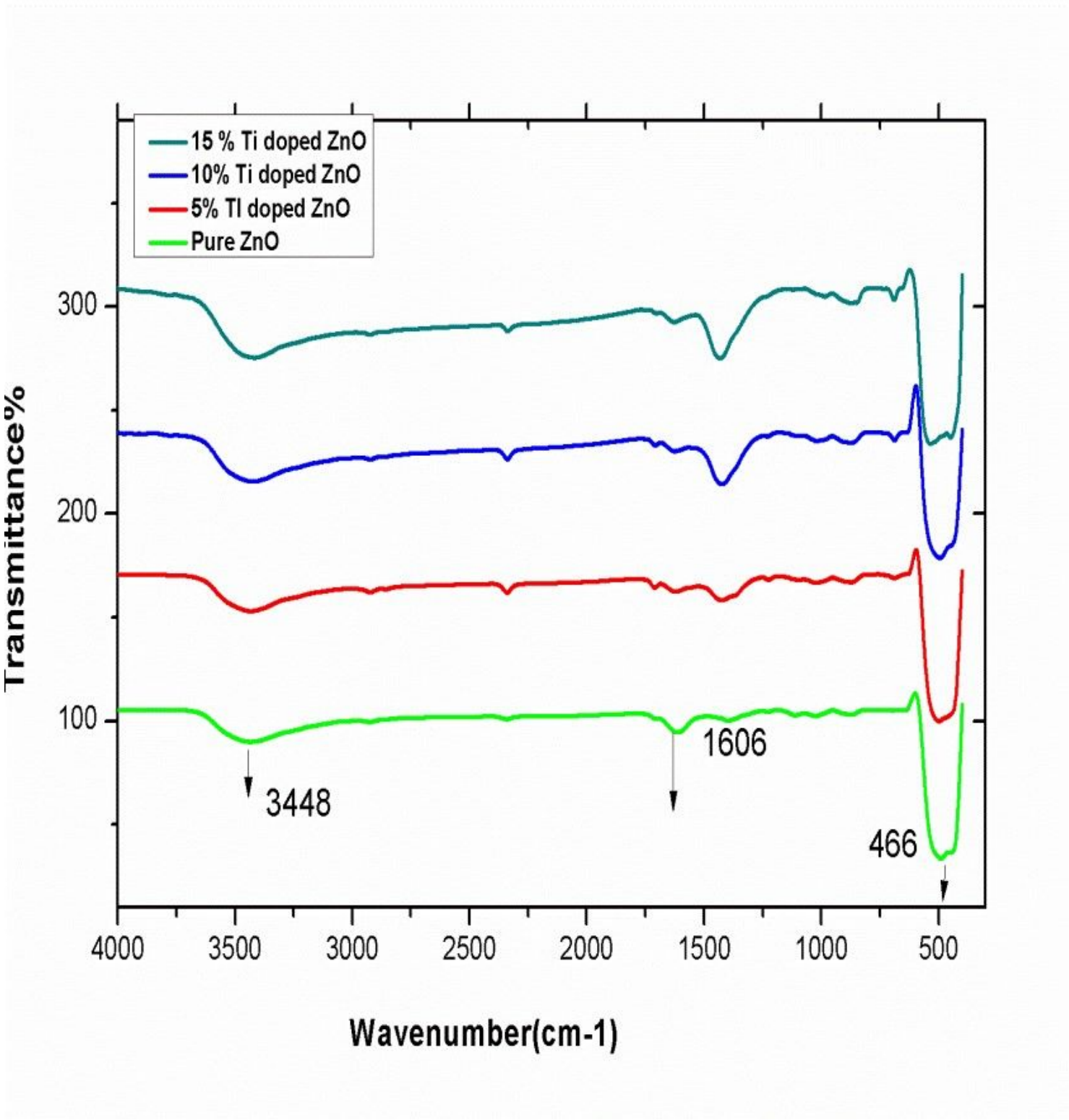

Figure 3

FTIR spectra of Ti x Zn1-xO (x= 0.00, 0.05, 0.10, 0.15)

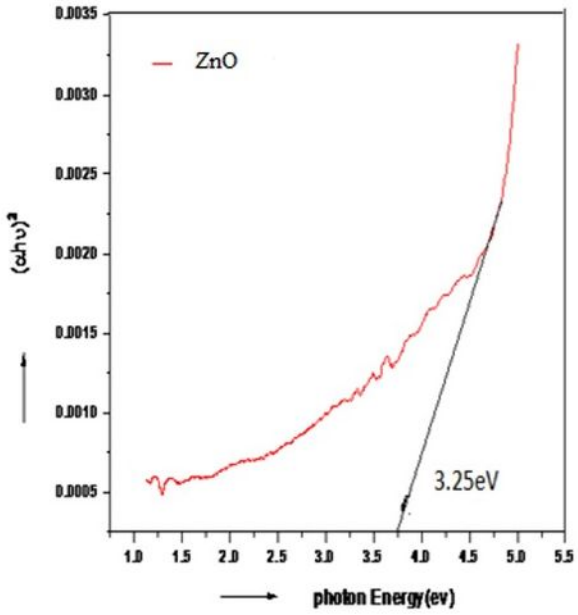

(a) Pure ZnO

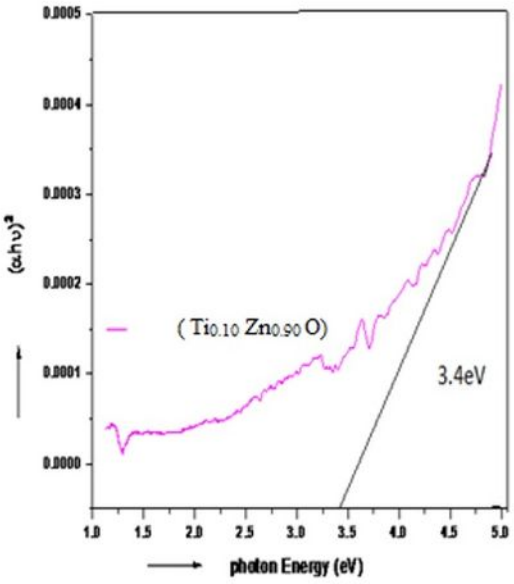

(c) 10 % Ti doped ZnO

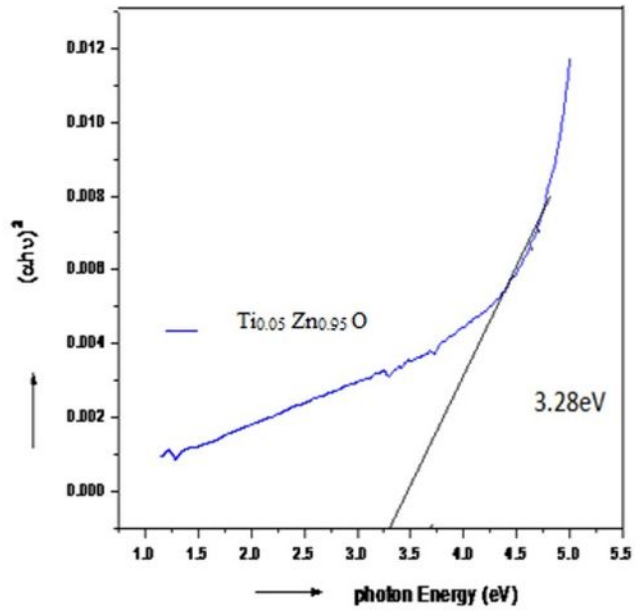

(b) 5 % Ti doped ZnO

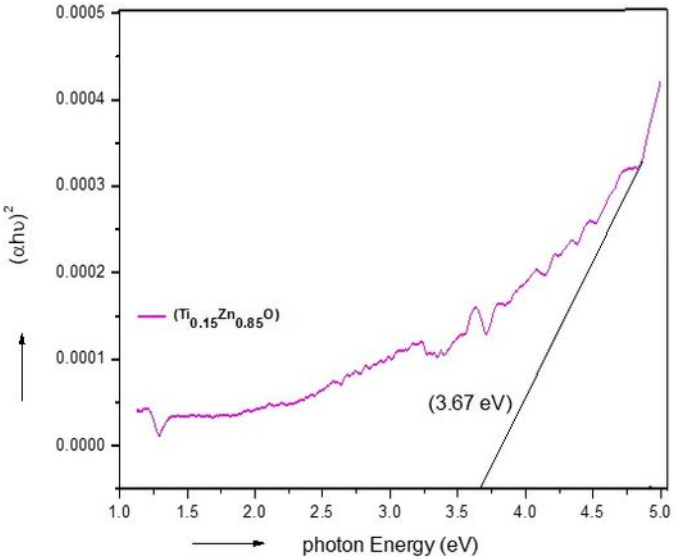

(d) 15 % Ti doped ZnO

Figure 4

Tauc's plot of Ti x Zn1-xO (x= 0, 0.05, 0.10 & 0.15)

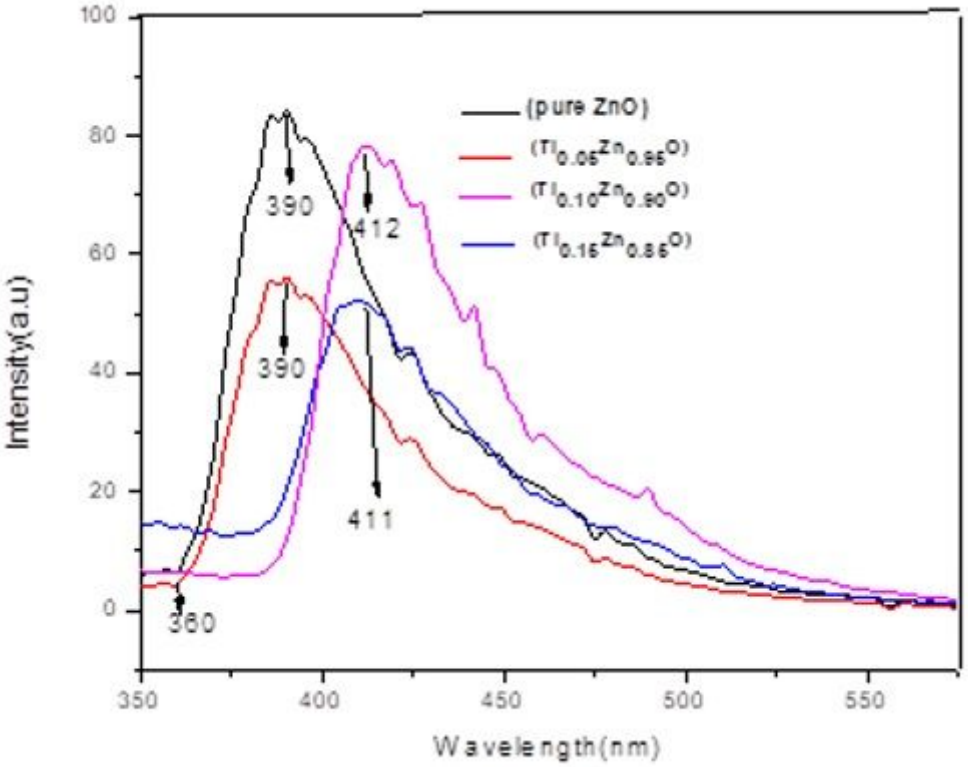

Figure 5

PL spectra of Ti x Zn1-xO (x= 0.00, 0.05, 0.10, 0.15)

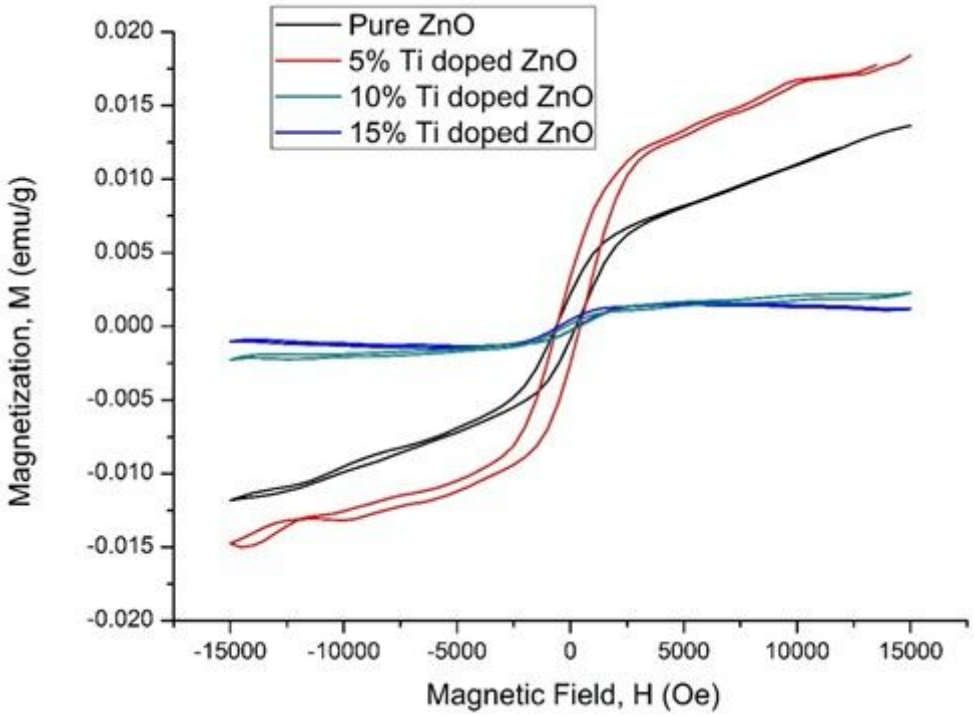

Figure 6

Hysteresis loop of Ti x Zn1-xO (x= 0.00, 0.05, 0.10, 0.15)